

## ROTATION OF JETS FROM YOUNG STARS: NEW CLUES FROM THE *HUBBLE SPACE TELESCOPE* IMAGING SPECTROGRAPH<sup>1</sup>

DEIRDRE COFFEY,<sup>2</sup> FRANCESCA BACCIOTTI,<sup>3</sup> JENS WOITAS,<sup>4</sup> THOMAS P. RAY,<sup>2</sup> AND JOCHEN EISLÖFFEL<sup>4</sup>

Received 2003 December 9; accepted 2003 December 12

### ABSTRACT

We report findings from the first set of data in a current survey to establish conclusively whether jets from young stars rotate. We observed the bipolar jets from the T Tauri stars TH 28 and RW Aur and the blueshifted jet from T Tauri star LkH $\alpha$  321, using the *Hubble Space Telescope* Imaging Spectrograph. Forbidden emission lines show distinct and systematic velocity asymmetries of 10–25 ( $\pm 5$ ) km s<sup>-1</sup> at a distance of 0".3 from the source, representing a (projected) distance of  $\approx 40$  AU along the jet in the case of RW Aur,  $\approx 50$  AU for TH 28, and 165 AU in the case of LkH $\alpha$  321. These velocity asymmetries are interpreted as rotation in the initial portion of the jet where it is accelerated and collimated. For the bipolar jets, both lobes appear to rotate in the same direction. Values obtained were in agreement with the predictions of MHD disk-wind models. Finally, we determine, from derived toroidal and poloidal velocities, values for the distance from the central axis of the footpoint for the jet's low-velocity component of  $\approx 0.5$ –2 AU, consistent with the models of magnetocentrifugal launching.

*Subject headings:* ISM: jets and outflows — stars: formation — stars: individual (LkH $\alpha$  321, RW Aurigae, TH 28) — stars: pre-main-sequence

### 1. INTRODUCTION

A key question in star formation research concerns the mechanisms behind the launch of jets from young stars. These jets are believed to play an important role in the removal of excess angular momentum from the system, thus allowing accretion of matter onto the star up to its final mass. It is generally acknowledged that magnetocentrifugal forces are responsible for jet launching. In particular, in the so-called disk-wind model (e.g., Ferreira 1997; Königl & Pudritz 2000) the jet is launched from the disk surface within a few AU from the star, while in the “X-wind” model (Shu et al. 2000) the base of the flow is located at a few stellar radii from the source. To date, resolution constraints on observations have impeded progress in validating the magnetocentrifugal mechanism, since jet launching occurs on small scales (i.e., less than 20 AU from the star); moreover, infall and outflow kinematics are complex and confused close to the source, which is often heavily embedded. Recently, however, interesting results have been obtained from observations of jets from more evolved, less embedded T Tauri stars (TTs) for which the jet can be optically traced back to its origin.

Observational backing for canonical models would require, for example, proof of rotation around the symmetry axis, close to the base where the jet is launched. The first hint of jet rotation was reported for the HH 212 system (Davis et al. 2000). However, the knots were located at  $2 \times 10^3$ – $10^4$  AU from the jet source. Independently, asymmetries in velocities

within the first 110 AU of the outflow from the T Tauri star DG Tau were found (Bacciotti et al. 2002), indicative of rotation. These results were obtained through an analysis of high angular resolution spectra taken with the *Hubble Space Telescope* Imaging Spectrograph (*HST*/STIS), aimed at probing the acceleration and collimation region of a stellar jet. Further confirmation of the rotation hypothesis came from Owens Valley Radio Observatory (OVRO) observations, which report the sense of rotation of the disk of DG Tau to be the same as that of the jet (Testi et al. 2002). Moreover, the derived toroidal velocities in the observed portion of the jet were seen to be in agreement with the predictions of the magnetocentrifugal models, and indeed they can be used to find the location on the disk plane of the launching point of the wind (Bacciotti et al. 2002; Anderson et al. 2003; Dougados et al. 2003; Pesenti et al. 2003).

These results motivated us to conduct an optical STIS survey to establish conclusively whether jets from young stars rotate. We report findings for another three sources (of eight in the survey sample; Table 1) for which the data have already been acquired, i.e., the bipolar jets from the TTs TH 28 and RW Aur and the blueshifted jet from LkH $\alpha$  321.

### 2. OBSERVATIONS

Observations were made of the jets associated with TH 28, LkH $\alpha$  321, and RW Aur using *HST*/STIS on 2002 June 22, August 20, and October 3, respectively (proposal ID 9435). An aperture of  $52 \times 0.1$  arcsec<sup>2</sup> was used with the G750M grating, which gave a spectral sampling of 0.554 Å pixel<sup>-1</sup>, corresponding to a radial velocity of  $\approx 25$  km s<sup>-1</sup> for the wavelength range covered. The angular sampling was 0".05 pixel<sup>-1</sup>. An acquisition of the stellar peak intensity prior to science observations allowed the slit to be centered accurately on the star before being offset to a position perpendicular to the jet axis at 0".3 from the source. We assume inclination angles (with regard to the plane of the sky) of 10° for TH 28 (Krautter 1986), 44° for RW Aur (López-Martín, Cabrit, & Dougados 2003), and 45° for LkH $\alpha$  321 (arbitrary, since unknown, although it may

<sup>1</sup> Based on observations made with the NASA/ESA *Hubble Space Telescope*, obtained at the Space Telescope Science Institute, which is operated by the Association of Universities for Research in Astronomy, Inc., under NASA contract NAS5-26555.

<sup>2</sup> Dublin Institute for Advanced Studies, 5 Merrion Square, Dublin 2, Ireland; dac@cp.dias.ie, tr@cp.dias.ie.

<sup>3</sup> INAF–Osservatorio Astrofisico di Arcetri, Largo E. Fermi 5, 50125 Florence, Italy; fran@arcetri.astro.it.

<sup>4</sup> Thüringer Landessternwarte Tautenburg, Sternwarte 5, 07778 Tautenburg, Germany; woitas, jochen@tls-tautenburg.de.

TABLE 1  
 SOURCES STUDIED IN THIS PAPER

Star	Location	Distance (pc)	Associated Outflow	$M_{\text{star}}$ ( $M_{\odot}$ )	$i_{\text{jet}}$ (deg)	$\dot{M}_{\text{disk}}$ ( $M_{\odot} \text{ yr}^{-1}$ )	$\dot{M}_{\text{jet}}$ ( $M_{\odot} \text{ yr}^{-1}$ )	$P_{\text{jet}}$ ( $M_{\odot} \text{ yr}^{-1} \text{ km s}^{-1}$ )	References
TH 28.....	Lupus 3	170	HH 228	...	10	...	$3.4 \times 10^{-8}$	$7.5 \times 10^{-6}$	1, 2
RW Aur.....	Auriga	140	HH 229	$\sim 1$	44	$10^{-6}$	$1.1 \times 10^{-7}$	$3.8 \times 10^{-5}$	3, 4
LkH $\alpha$ 321.....	Cygnus	550	HH 421	...	...	...	...	...	5

NOTES.—Where known, the table also lists the mass of the star, the jet inclination angle ( $i_{\text{jet}}$ ) with respect to the plane of the sky, the mass accretion rate through the disk ( $\dot{M}_{\text{disk}}$ ), and the fluxes of mass ( $\dot{M}_{\text{jet}}$ ) and poloidal momentum ( $P_{\text{jet}}$ ) in the jet.

REFERENCES.—(1) Bacciotti & Eisloffel 1999; (2) Krautter 1986; (3) Woitas et al. 2002; (4) López-Martín et al. 2003; (5) Mundt & Eisloffel 1998.

have a large inclination angle from spectroastrometric measurements; Whelan et al. 2003). The offset of  $0''.3$  then represents a deprojected distance of  $\approx 51$ , 195, and 233 AU along the jet for TH 28, RW Aur, and LkH $\alpha$  321, respectively. The only exception was in the case of the RW Aur blueshifted jet lobe, where the slit was placed at  $0''.2$  because of lack of line emission at  $0''.3$  (Woitas et al. 2002). Spectra were obtained of the blue- and redshifted lobes, using exposure times of 2200 and 2700 s, respectively, for the bipolar jets associated with TH 28 and RW Aur. In the case of LkH $\alpha$  321, only the blueshifted lobe was detectable, and so two spectra of this lobe, with exposure times of 2200 and 2700 s, were obtained and summed to increase the signal-to-noise ratio of the faint emission lines. In total, this yielded five spectra, in the transverse direction at the base of the jets, which included H $\alpha$  and the forbidden emission lines [O I]  $\lambda\lambda 6300, 6363$ , [N II]  $\lambda\lambda 6548, 6583$ , and [S II]  $\lambda\lambda 6716, 6731$ . Data were calibrated through the standard *HST* pipeline, subtraction of the reflected stellar continuum was performed, and hot/dark pixels were removed.

### 3. RESULTS

In order to determine whether rotation is present in the jet channel, the difference in velocities on either side of the jet axis was analyzed. Position-velocity contour plots for a sample of emission lines are shown in Figure 1 (*top panels*). All radial velocities are systemic, i.e., they are quoted with respect to the mean heliocentric velocity of the star, which has been measured from photospheric lines to be  $+5 \text{ km s}^{-1}$  for TH 28 (Graham & Heyer 1988),  $+23 \text{ km s}^{-1}$  for RW Aur (Woitas et al. 2003), and  $-7 \text{ km s}^{-1}$  for LkH $\alpha$  321 (E. Whelan 2003, private communication). The lower order contours trace the outer jet channel where the jet is not so well collimated and where the lower velocities lie. If rotation is present, there will be a difference in radial velocities between the two sides of the jet. This difference will be evident graphically as a skew in the contours of the transverse position-velocity diagram. Such a skew is indeed observed in all three cases in the outer contour lines. This suggests the presence of rotation in at least the low-velocity component (LVC) of the flow near the outer borders of the jet channel. The high-velocity component (HVC), which is located much closer to the jet axis and gives rise to the emission peak (Bacciotti et al. 2000), appears not to be spatially resolved in our spectra. For this reason we cannot resolve any velocity difference in the HVC between the two sides of the flow, i.e., we cannot detect rotation for this velocity component.

To give a quantitative estimate of the observed velocity shifts, it was firstly necessary to ensure that we measure velocity offsets at equal distances on either side of the jet axis. To this purpose we assumed that the peak of the (HVC) emission traces the position of the axis and measured its

distance from the nominal center of the slit, with a Gaussian fit along the cross-dispersion direction. We then shifted the line emission, recentering the HVC peak on the nominal  $0''$  position. In all cases a small offset ( $\leq 0.4$  pixels) was required (Table 2). The offsets have different sign and magnitude for the three targets, indicating that this is not an instrumental systematic effect. Instead, pixel-shift values for emission lines in opposite jet lobes are consistent with a maximum misalignment  $\leq 2^\circ$  with respect to the perpendicular of the actual jet axis at subarcsecond scales. This resulted in a displacement of the peak intensity of up to  $0''.02$ , a quantity that would produce a marginal asymmetry in radial velocity estimated to be at most 20% if uncorrected (Bacciotti et al. 2002). This error was, however, avoided since the emission was brought on-axis prior to analysis.

The peak intensities of pixel rows on either side of the central row were then compared for velocity differences, Figure 1 (*bottom panels*). The intensity profiles of each pair of pixel rows symmetric about the jet axis was plotted (e.g.,  $\pm 0''.1$ , or as indicated in each box). The single curve at the bottom in each case is the intensity of the central on-axis pixel row. Two methods were used in velocity measurements: a cross-correlation technique, which analyses the overall displacement of lines and is independent of the shape of the line profile; and a Gaussian fitting technique, which acts as a suitable check given the simple shape of the line profile in most cases. Specifically, each pair of pixel rows, mirrored in distance from the jet axis, was cross-correlated, and Gaussian fits for each pair of rows were also compared. The outcomes of the two methods are consistent, showing clear radial velocity differences of 10–25 ( $\pm 5$ )  $\text{km s}^{-1}$  for opposing jet edges. Results are listed in Table 3, in which we report the measured radial velocity differences in the direction of the oriented slit, corresponding to a direction specified in the first column of the table. In a small number of cases, flagged in the table with asterisks, the emission had to be filtered out of a background that was causing velocity measurements to be artificially changed because of relatively strong HVC presence, oversubtraction of the background, or a low signal-to-noise ratio at crucial positions. The overall results are illustrated graphically in Figures 2–4.

Finally, the radial velocity profile across each jet is shown in Figure 5. In the redshifted lobes of TH 28 and RW Aur, the on-axis radial velocity is clearly the highest and the value reduces as the edges of the jet are approached. The blueshifted lobes are not so clear since the emission is fainter and often more scattered. Data reduction in these cases often required isolation of the lower velocity component from the HVC (as marked in Table 3) to identify elements of rotation. However, radial velocities in this figure *include* the HVC, and so rotation is not apparent in all cases.

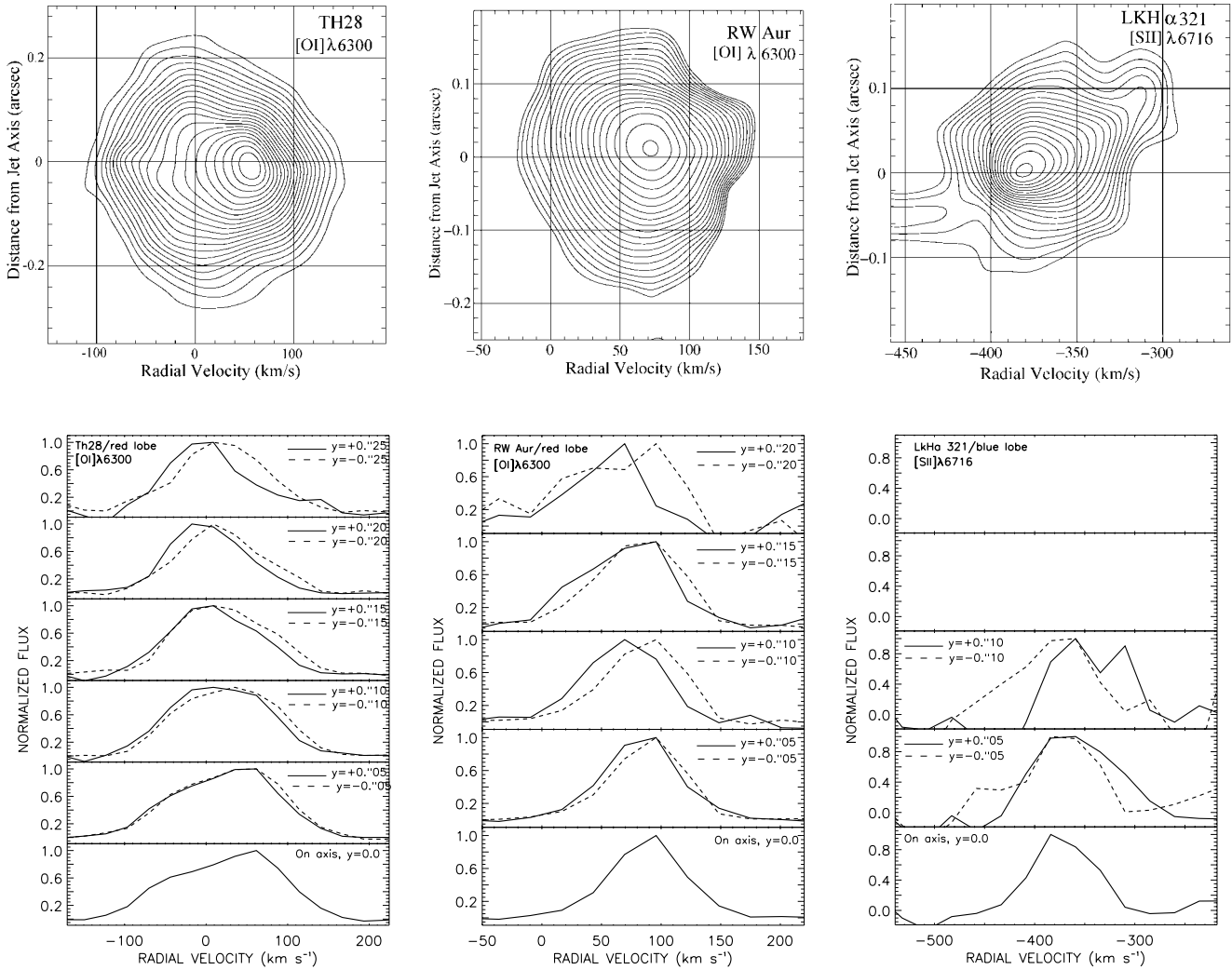


FIG. 1.—*Top panels:* Selected position-velocity contour plots of emission lines from the studied jets. The skew in lower order contours is indicative of rotation in the outer jet channel, while the high-velocity component remains unresolved. Contour values in units of  $\text{ergs cm}^{-2} \text{s}^{-1} \text{\AA}^{-1} \text{arcsec}^{-2}$  in the panels are as follows: TH 28 is from  $7.0 \times 10^{-15}$  to  $6.7 \times 10^{-14}$ , with intervals of  $3.0 \times 10^{-15}$ ; RW Aur is from  $7.2 \times 10^{-15}$  to  $2.3 \times 10^{-13}$ , log scale interval of  $2^{1/4}$ ; and LkH $\alpha$  321 is from  $1.0 \times 10^{-15}$  to  $8.2 \times 10^{-15}$ , with intervals of  $4.0 \times 10^{-16}$ . Panels are corrected for the heliocentric velocity of the star, that is, for +5, +23, and  $-7 \text{ km s}^{-1}$  in the three cases, respectively. *Bottom panels:* Normalized intensity profiles along horizontal cuts in the above panels, symmetrically opposed with respect to the jet axis.

From the results of this spectral analysis, combined with the inclination angles, for the RW Aur jet we find poloidal velocities of  $144\text{--}227 \text{ km s}^{-1}$  in the red lobe and  $245\text{--}288 \text{ km s}^{-1}$  in the blue lobe (this velocity asymmetry is well known from previous observations; Woitas et al. 2002), for TH 28 jet we find  $115\text{--}288 \text{ km s}^{-1}$  in the red lobe and  $230\text{--}374 \text{ km s}^{-1}$  in the blue lobe (an asymmetry that was also previously recorded; Graham & Heyer 1988), and for LkH $\alpha$  321 we find  $540\text{--}550 \text{ km s}^{-1}$ . Toroidal velocities derived from the outer positional radial velocity shifts, being less affected by projection effects (see § 4), are in the ranges of  $7\text{--}17 \text{ km s}^{-1}$  for both lobes of RW Aur,  $5\text{--}13 \text{ km s}^{-1}$  for the red lobe of TH 28,  $4\text{--}8 \text{ km s}^{-1}$  for the blue lobe of TH 28, and  $4\text{--}9 \text{ km s}^{-1}$  for the blue lobe of LkH $\alpha$  321. (Note that in the ranges given above, the higher poloidal velocities lie at distances closest to the rotation axis, and these correspond to the lower toroidal and radial velocities.)

#### 4. DISCUSSION

Assuming that emission from the jet is axially symmetric, we interpret our findings of velocity differences between the

two sides of the jet flow (Table 3 and Figs. 2–4) as evidence for rotation at the base of the jet. Most importantly, for TH 28 and RW Aur, the red and blue jet lobes were found to rotate in the same direction. This implies that the helicity in the red and blue lobes (i.e., the handedness of toroidal with respect to the poloidal velocity) is opposite in opposite directions, a result predicted by MHD models where the ambient field is wrapped around because of disk rotation.

Before looking at each target individually, there are a few general comments to be made about the results in Table 3. First, the velocity difference measurements close to the jet axis, i.e., at the  $0^{\circ}05$  position, are noticeably smaller than points farther away, and where the emission is detectable at  $0^{\circ}2$  and beyond, velocity differences are higher than at intermediate distances. This effect may at first appear to contradict the notion that the central portions of the jet should rotate faster. A detailed comparison with disk-wind model predictions (Pesenti et al. 2003; Dougados et al. 2003) shows, however, that the apparent decrease of the observed velocity difference toward the jet axis is likely due to projection and beam-smearing effects. Since the emission is optically thin, we

TABLE 2  
PIXEL SHIFTS

Jet Lobe	Pixel Shift Applied
TH 28 red lobe .....	+0.3672
TH 28 blue lobe.....	-0.3672
RW Aur red lobe.....	-0.216
RW Aur blue lobe.....	+0.1728
LkH $\alpha$ 321 blue lobe.....	-0.36

NOTES.—Pixel shifts are applied to emission lines in each jet lobe along the cross-dispersion direction to recenter the HVC emission peak, assumed to be coincident with the jet axis, on the nominal  $0''$  position.

see, along the line of sight, the sum of the contributions emitted from regions in the jet that rotate with different toroidal velocities. This causes a reduction of the observed velocity shift. Such an effect is more important for regions closer to the axis, while the values measured at the outer jet borders are less contaminated and so are in better agreement with theoretically predicted toroidal velocities. In other words, this effect does not reflect a true kinematic feature but is expected on the basis of MHD acceleration models when combined with our observational mode. Second, it should be noted that the size of velocity differences in different emission lines does not represent scattering around an average value but rather is due to the fact that emission has its origin at different positions along the line of sight. And lastly, the [N II] lines show higher velocity differences than other emission lines, a result that illustrates how they trace the central more collimated higher velocity region of the flow (see Bacciotti et al. 2000; López-Martín et al. 2003; Pesenti et al. 2003).

The results for the TH 28 redshifted jet lobe are clearest. Velocity differences in the southwest-northeast direction are positive, with a few exceptions mainly in the [S II] lines.

Also, the data close to the jet axis are not well resolved, as explained above. The stronger [O I] and [N II] lines have values of 5 and 6 km s<sup>-1</sup> at  $0''05$  from the axis, compared with 10–20 km s<sup>-1</sup> farther from the axis, while the outer jet channel seems to have higher radial velocity differences of about 24 km s<sup>-1</sup>. Values in the blueshifted jet lobe are less clear, but [N II] and [O I] emission gives positive differences consistent with the redshifted lobe. All other usable data points fall within the error bars about zero. Globally, we find evidence that both lobes of the jet rotate in a clockwise direction, looking down the blueshifted jet lobe toward the source, with a measured radial velocity difference of 10–25 km s<sup>-1</sup>.

The RW Aur jet also shows clear indications of rotational velocities. Exceptions include the [S II]  $\lambda 6731$  values in the redshifted lobe. Also, points close to the jet axis show smaller radial velocity differences due to strong unresolved HVC emission. However, the [O I] lines give clear results, with higher radial velocity difference evident at  $0''2$  from the jet axis. The blueshifted lobe is less definite, but nevertheless velocity differences outside the error bars are positive in line with the redshifted lobe. Overall, results show an anticlockwise rotation looking down the blueshifted jet lobe toward the source, again with radial velocity differences of 10–25 km s<sup>-1</sup>. These findings are consistent in magnitude and direction with results of similar research on the RW Aur jet (Woitak et al. 2003) in which rotational velocities in the same direction of 10–20 km s<sup>-1</sup> have been observed, in the form of velocity differences between the borders of the flow. For this study *HST*/STIS was also used, but the spectra were taken in a set of positions across the jet with the slit direction parallel to the jet axis.

In the case of LkH $\alpha$  321, which is located at 550 pc (more than 3 times the distance of the other targets), the emission lines were very faint despite having combined two spectra to increase the signal-to-noise ratio. Nevertheless,

TABLE 3  
RADIAL VELOCITY DIFFERENCES

Jet Lobe	Distance from Jet Axis (arcsec)	$\Delta V_{\text{rad}}$ for [O I] $\lambda 6300$ (km s <sup>-1</sup> )	$\Delta V_{\text{rad}}$ for [O I] $\lambda 6363$ (km s <sup>-1</sup> )	$\Delta V_{\text{rad}}$ for [N II] $\lambda 6548$ (km s <sup>-1</sup> )	$\Delta V_{\text{rad}}$ for H $\alpha$ $\lambda 6563$ (km s <sup>-1</sup> )	$\Delta V_{\text{rad}}$ for [N II] $\lambda 6583$ (km s <sup>-1</sup> )	$\Delta V_{\text{rad}}$ for [S II] $\lambda 6716$ (km s <sup>-1</sup> )	$\Delta V_{\text{rad}}$ for [S II] $\lambda 6731$ (km s <sup>-1</sup> )
TH 28, redshifted (southwest-northeast) .....	0.05	5	...	21*	...	6	-5	-4
	0.1	12	...	30*	...	14	-1	1
	0.15	11	...	30*	...	21	3	3
	0.2	16	...	32*	...	25	8	7
	0.25	23	...	...	...	...	10	-1
TH 28, blueshifted (southwest-northeast) .....	0.05	2*	...	1	...	5	...	...
	0.1	3*	...	...	...	8	...	...
	0.15	8	...	...	...	7	...	...
	0.2	15	...	...	...	...	...	...
RW Aur, redshifted (northeast-southwest).....	0.05	7	5	...	...	14	1	-1
	0.1	20	14	...	...	...	-4	-5
	0.15	10	...	...	...	...	...	2
	0.2	24	...	...	...	...	...	...
RW Aur, blueshifted (northeast-southwest).....	0.05	...	6*	...	...	-5*	12	4*
	0.1	...	...	...	...	15*	25	14*
	0.15	...	...	...	...	...	...	...
LkH $\alpha$ 321, blueshifted (northwest-southeast) .....	0.05	...	-8*	...	4*	3*	-12*	3*
	0.1	...	...	...	-7*	-5*	-31*	...

NOTES.—Radial velocity differences,  $\Delta V_{\text{rad}}$ , across the jet  $0''3$  from the source ( $0''2$  for the RW Aur blue lobe), measured using both the cross-correlation technique and single-Gaussian fitting, along the direction specified in the first column. The asterisks mark data points that have been filtered out of a low signal-to-noise environment, or from a strong spurious contribution from the HVC emission wings. Where ellipses appear in the table, the emission was either shifted off the CCD, or was too faint, small or scattered to decipher. The accuracy reached with the data analysis is approximately  $\pm 5$  km s<sup>-1</sup>.

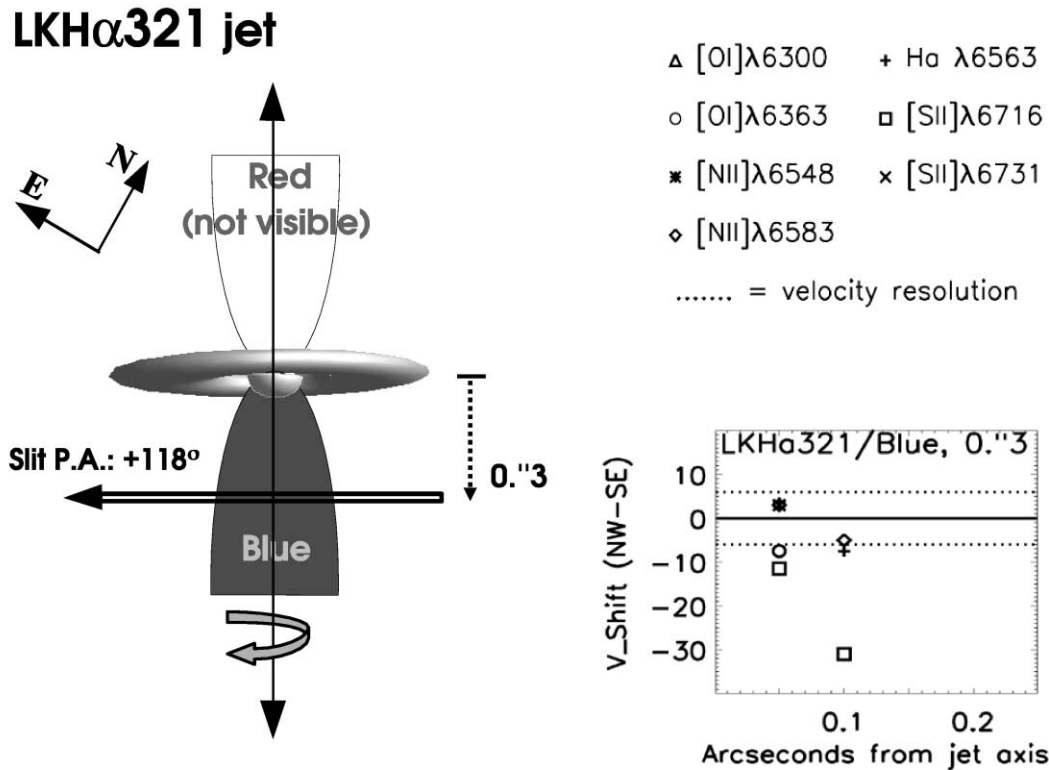


FIG. 2.—*Left*: Schematic drawing of the observing mode for the blueshifted jet from LkH $\alpha$  321. The derived sense of rotation is illustrated by the circular arrow around the symmetry axis. *Top right*: Symbols adopted for the various lines. *Bottom right*: Summary of radial velocity asymmetries measured at the base of the blueshifted lobe, at 0."3 from the source, in the direction of the oriented slit, i.e., northwest-southeast (also specified by the label of the y-axis).

velocity differences in the range of  $-5$  to  $-30$  km s $^{-1}$  have been measured, although evidence of rotation is weaker in this case. The sense of rotation for LkH $\alpha$  321 is measured as anticlockwise looking down the blueshifted lobe toward the star. In this jet we are able to measure rotation at higher velocities because of a number of factors: LkH $\alpha$  321 is farther away, meaning that we are looking farther along the jet (233 AU from the source, deprojected distance) to a point where it has widened, and so we can resolve higher velocities; a large inclination angle (which appears to be the case from spectroastrometric measurements; Whelan et al. 2003) would mean that the poloidal and radial velocities approach each other; and finally, this is a larger mass T Tauri star, since it has spectral type G1 (Chavarría-K. et al. 1981), implying higher velocities in the outer resolvable regions of the jet.

It is reassuring that we obtain *negative* shifts in the case of LkH $\alpha$  321, as opposed to the positive shifts observed for the other two sources because, as we are comparing the *same* rows on the CCD detector in all cases, it means we are not measuring an instrumental effect. Conceivably, a slight misalignment of the slit with respect to the transverse direction of the jet (i.e., an inaccurate position angle used in the pointing of the instrument) may produce an effect similar to rotation. In this case, the position of the real jet axis will then be shifted with respect to the nominal 0" position. We have shifted the spectral image back to the 0" position as previously discussed (§ 3), but the angle subtended remains a problem. It could produce a rotation signature even in a nonrotating jet, since the HVC and LVC are at different spatial locations on the CCD with respect to the 0" row of pixels, implying that we are not probing symmetric regions of the jet with respect to its

real axis. Given that such a misalignment has occurred, the extent of the contamination does not have, however, a dramatic affect on our results, as can be seen from the fact that the pixel-shift requirements for TH 28 and LkH $\alpha$  321 (Table 2) are in the same direction but the sense of rotation of their jets is opposite. For RW Aur, the same position angle was used here for slit positioning as in a previous study (Woitak et al. 2003), where it was found that the magnitude of the false rotation signature contamination due to incorrect position angle was, at most, 1–5 km s $^{-1}$ . However, the sense of the false signature is in fact opposite in direction to that of the jet's rotation, and so the values we have measured are actually lower limits. Apart from this, the only other obvious effect that could produce a contour skew mimicking rotation is asymmetrical interaction with the local environment on either side of the propagating jet, e.g., asymmetrical mass entrainment leading to asymmetrical poloidal velocities. However, such mimicking is unlikely because (apart from the fact that asymmetrical entrainment should also produce enhanced emission at one border of the flow, which is not seen in our spectra) we see the same asymmetry in both the red- and blueshifted jet lobes where present, and the magnitudes of the deduced toroidal velocity differences are in the range predicted by theory (as discussed below).

Overall, our observations are in line with the observations of the jet from the T Tauri star DG Tau (Bacciotti et al. 2002). In that case, by using simple and general relationships governing the physics of magnetically launched disk winds together with an observationally based estimate of the ratio,  $R$ , between the mass flux in the jet and the mass flux accreted through the disk ( $R \sim 0.1$ ), it was demonstrated that the observed velocity

### TH 28 jet

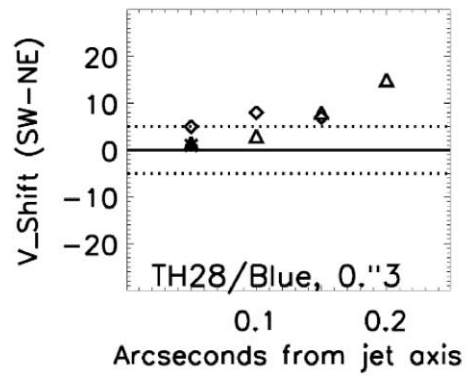
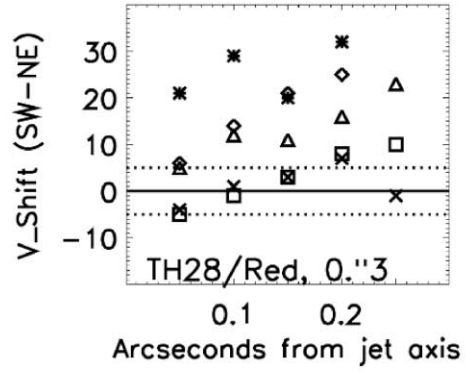
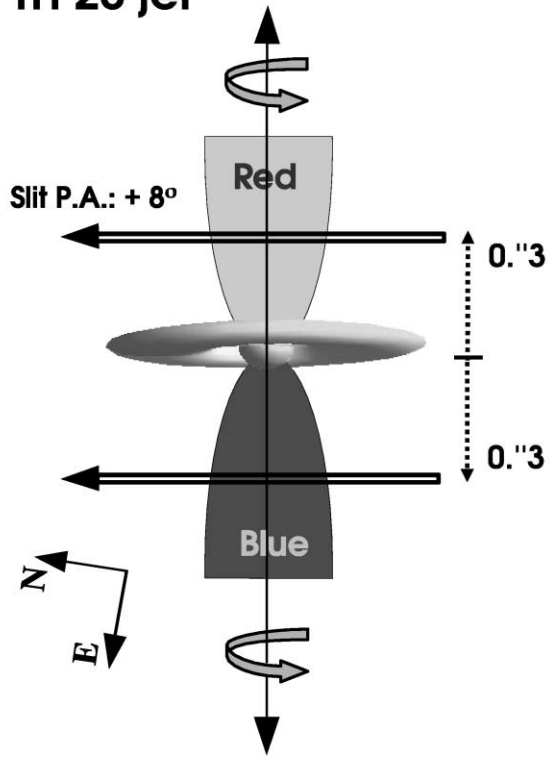


FIG. 3.—Same as Fig. 2, for the bipolar jet from TH 28. Both slits were located at  $0".3$  from the source.

### RW Aur jet

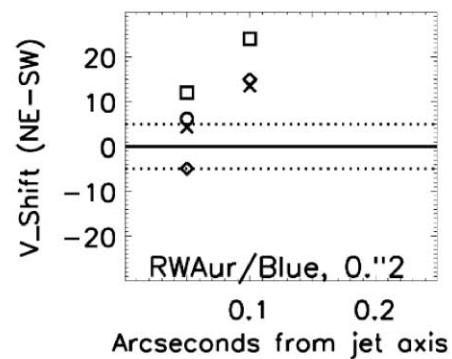
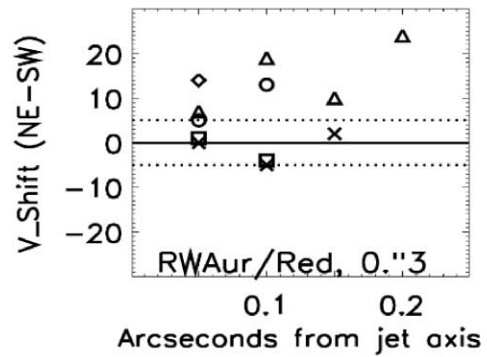
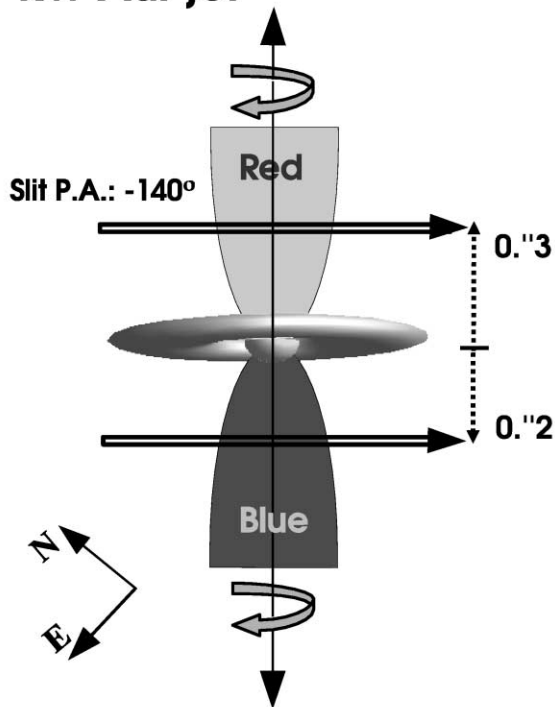


FIG. 4.—Same as Fig. 2, for the bipolar jet from RW Aur. In the blueshifted jet lobe the spectrum was taken at  $0".2$  from the star.

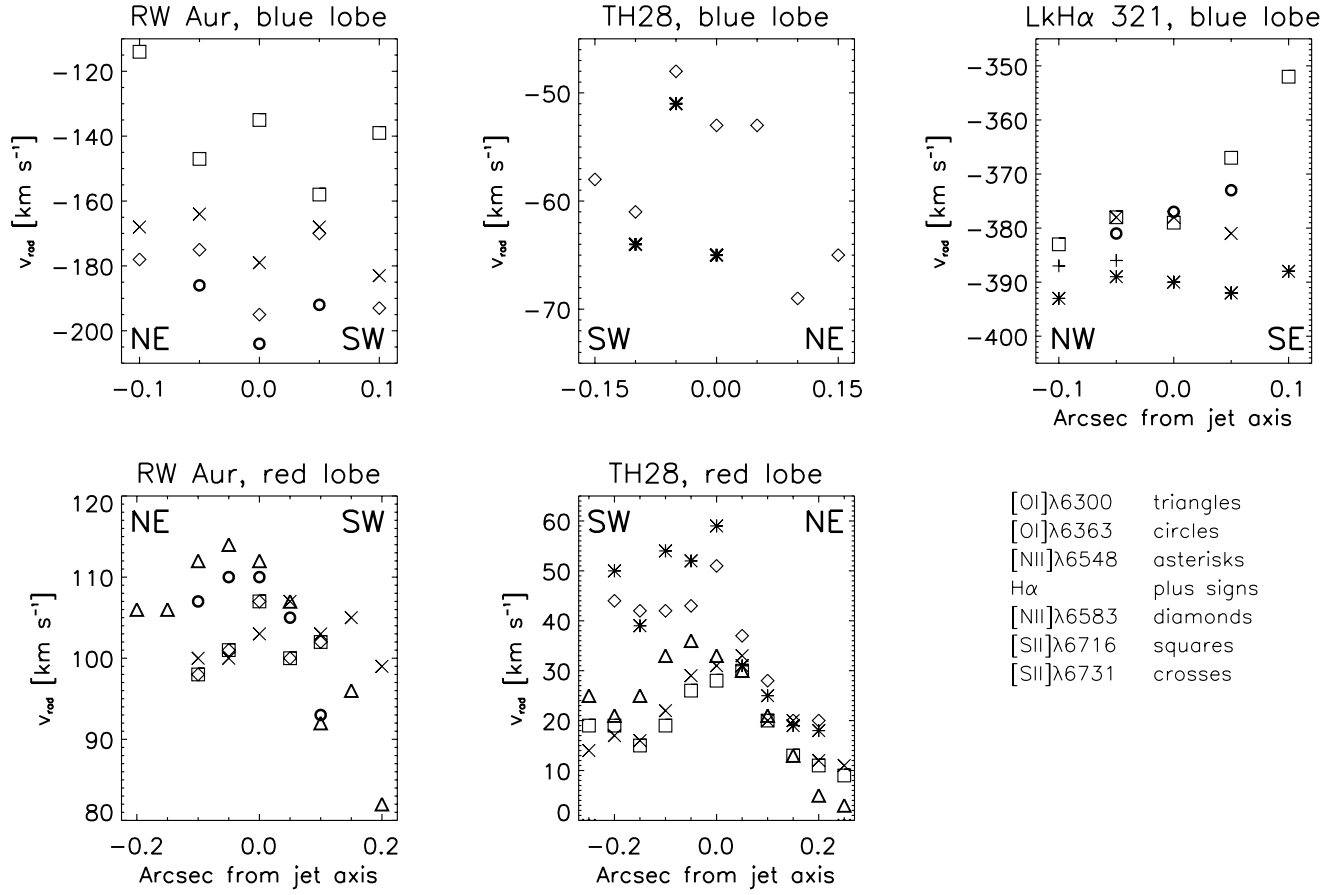


FIG. 5.—Radial velocity profile across each jet in various emission lines. The TH 28 blueshifted [O I]  $\lambda$ 6300 line is not included since the profile of this emission line is very wide and did not allow measurement of velocity peaks with Gaussian fitting. In this case the rotational velocities were derived from cross-correlation routines alone, resulting only in velocity difference measurements.

TABLE 4  
LAUNCH POINT OF THE DISK WIND

Star	Jet Lobe	$\varpi_{\infty}$ (arcsec)	$\varpi_{\infty}$ (AU)	$\Delta v_{\text{rad}}$ ( $\text{km s}^{-1}$ )	$v_{\text{rad}}$ ( $\text{km s}^{-1}$ )	$\varpi_0$ (AU)
TH 28	Redshifted	0–0.2	1–34	10–25	30–20	0.3–1.6
	Blueshifted	0.1–0.2	17–34	8–15	50–40	0.1–0.4
RW Aur	Redshifted	0.1–0.2	14–28	10–25	105–100	0.4–1.3
	Blueshifted	0.05–0.1	7–14	10–25	180–170	0.1 <sup>a</sup> –0.4
LkH $\alpha$ 321	Blueshifted	0.05–0.1	27.5–55	5–12	390–380	0.1 <sup>a</sup> –0.2

NOTES.—The range for the launch point of the disk wind,  $\varpi_0$ , for our five targets, calculated using the method described in Anderson et al 2003.

<sup>a</sup> Where emission is faint values for the 0<sup>o</sup>05 position were used, but these should be considered less accurate because of resolution constraints.

differences were in the expected range (Bacciotti et al. 2002; Anderson et al. 2003; Dougados et al. 2003). These values compare well with our results, which therefore support the magnetocentrifugal scenario. Furthermore, our toroidal and poloidal velocities have the same ratio as theoretical predictions (Vlahakis et al. 2000), and we can use these velocities,  $v_{\phi,\infty}$  and  $v_{p,\infty}$  measured at a distance,  $\varpi_\infty$ , from the rotation axis, to obtain values for the wind-launch region in terms of distance from the rotation axis along the disk plane,  $\varpi_0$ . Using equation (1) (Anderson et al. 2003),

$$\varpi_0 \approx 0.7 \text{ AU} \left( \frac{\varpi_\infty}{10 \text{ AU}} \right)^{2/3} \left( \frac{v_{\phi,\infty}}{10 \text{ km s}^{-1}} \right)^{2/3} \times \left( \frac{v_{p,\infty}}{100 \text{ km s}^{-1}} \right)^{-4/3} \left( \frac{M_*}{1 M_\odot} \right)^{1/3}, \quad (1)$$

and assuming all three sources are of mass  $M_* \sim 1 M_\odot$ , which is a reasonable approximation given the weak dependence on  $M_*$ , we obtain values for  $\varpi_0$  as shown in Table 4. We have chosen measurements at  $0''.1$  and  $0''.2$  from the jet axis as limits of a suitable range, which are less contaminated by projection effects. Where emission was faint, values corresponding to  $0''.05$  were used, but it should be noted that these are less accurate. Also, the values at  $0''.1$  are less precise than those at  $0''.2$ , when both are present, since increased projection effects close to the jet axis tend to reduce the line-of-sight averaged  $v_{\phi,\infty}$  and hence the resulting value of  $\varpi_0$  (Pesenti et al. 2003). Considering the redshifted jet lobes, which both have very strong signal-to-noise ratio in [O I] and [N II] emission lines, we calculate a wind-launch region spanning 0.3–1.6 AU, in keeping with previous estimates for DG Tau of  $\sim 1.8$  AU (Bacciotti et al. 2002) and  $\sim 0.3$ –4 AU (Anderson et al. 2003). The observational evidence presented here supports the idea that disk winds are launched, via the magnetocentrifugal mechanism (e.g., Königl & Pudritz 2000), at radii within a few AU of the star. Determination of the most appropriate model, however, will have to await higher spatial and spectral resolution observations in the future.

## 5. CONCLUSIONS

The jets from the three young stars observed, TH 28, RW Aur, and LkH $\alpha$  321, show distinct and systematic radial velocity asymmetries in opposing positions with respect to the jet axis, at  $0''.2$ – $0''.3$  from the source. Although the on-axis higher velocity component of the jet remains unresolved, radial velocity differences in the lower velocity component located in the outer jet channel are found to be on the order of 10–25 ( $\pm 5$ ) km s $^{-1}$ . For the bipolar jets from TH 28 and RW Aur, the velocity differences have the same sign in both lobes. We interpret these radial velocity asymmetries as rotation signatures in the region where the jet has been collimated but has not yet manifestly interacted with the environment. Therefore, the sense of rotation of the jets, looking down the blueshifted lobe toward the star, is clockwise for TH 28 and anticlockwise for RW Aur and LkH $\alpha$  321.

Our findings are reinforced in a number of ways: the velocity differences are of the same magnitude as those measured in the similar DG Tau jet of 5–10 km s $^{-1}$  (Bacciotti et al. 2002), which was shown to be in agreement with the predictions of MHD disk-wind models (Bacciotti et al. 2002; Anderson et al. 2003; Dougados et al. 2003; Pesenti et al. 2003); they are in line with similar research on the RW Aur jet (Woitas et al. 2003), which yields rotational velocities of 10–20 km s $^{-1}$ , with the same sense of rotation; and finally, they lead to values for the distance of the LVC footpoint from the central axis of  $\approx 0.5$ –2 AU, consistent with the models of magnetocentrifugal launching (Anderson et al. 2003).

We wish to thank Marcello Felli, Catherine Dougados, Emma Whelan, and Jonathan Ferreira for useful comments and suggestions. D. C. and T. P. R. would like to acknowledge support for their research from Enterprise Ireland, and J. E. and J. W. likewise wish to acknowledge support from the Deutsches Zentrum für Luft-und Raumfahrt under grant 50 OR 0009. We would also like to thank the anonymous referee for useful comments.

## REFERENCES

- Anderson, J. M., Li, Z.-Y., Krasnopolsky, R., & Blandford, R. 2003, *ApJ*, 590, L107
- Bacciotti, F., & Eisloffel, J. 1999, *A&A*, 342, 717
- Bacciotti, F., Mundt, R., Ray, T. P., Eisloffel, J., Solf, J., & Camezind, M. 2000, *ApJ*, 537, L49
- Bacciotti, F., Ray, T. P., Mundt, R., Eisloffel, J., & Solf, J. 2002, *ApJ*, 576, 222
- Chavarría-K., C., & de Lara, E. 1981, *Rev. Mexicana Astron. Astrofiz.*, 6, 159
- Davis, C. J., Berndsen, A., Smith M. D., Chrysostomou, A., & Hobson, J. 2000, *MNRAS*, 314, 241
- Dougados, C., Cabrit, S., Ferreira, J., Pesenti, N., Garcia, P., & O'Brien, D. 2003, *Ap&SS*, 287, 135
- Ferreira, J. 1997, *A&A*, 319, 340
- Graham, J. A., & Heyer, M. H. 1988, *PASP*, 100, 1529
- Königl, A., & Pudritz, R. 2000, in *Protostars and Planets IV*, V. Mannings, A. P. Boss, & S. S. Russell (Tucson: Univ. Arizona Press), 759
- Krautter, J. 1986, *A&A*, 161, 195
- López-Martín, L., Cabrit, S., & Dougados, C. 2003, *A&A*, 405, L1
- Mundt, R., & Eisloffel, J. 1998, *AJ*, 116, 860
- Pesenti, N., Dougados, S., Cabrit, S., Ferreira, J., Casse, F., Garcia, P., & O'Brien, D. 2003, *A&A*, submitted
- Shu, F. H., Najita, J. R., Shang, H., & Li, Z.-Y. 2000, in *Protostars and Planets IV*, V. Mannings, A. P. Boss, & S. S. Russell (Tucson: Univ. Arizona Press), 789
- Testi, L., Bacciotti, F., Sargent, A. I., Ray, T. P., & Eisloffel, J. 2002, *A&A*, 394, L31
- Vlahakis, N., Tsinganos, K., Sauty, C., & Trussoni, E. 2000, *MNRAS*, 318, 417
- Whelan, E. T., Ray, T. P., & Davis, C. J. 2003, *A&A*, submitted
- Woitas, J., Bacciotti, F., Ray, T. P., Marconi, A., Coffey, D., & Eisloffel, J. 2003, *A&A*, submitted
- Woitas, J., Ray, T. P., Bacciotti, F., Davis, C. J., & Eisloffel, J. 2002, *ApJ*, 580, 336